JOURNAL OF SPACECRAFT AND ROCKETS
Vol. 41, No. 2, March–April 2004

Preliminary Thermal–Mechanical Sizing of a Metallic Thermal Protection System

Carl C. Poteet*
NASA Langley Research Center, Hampton, Virginia 23681
and
Hasan Abu-Khajeel† and Su-Yuen Hsu†
Lockheed Martin Space Operations, Hampton, Virginia 23681

A process is developed to perform thermal and structural analysis and sizing and to perform sensitivity studies on the latest metallic thermal protection system developed at NASA Langley Research Center. The process defined can be used to determine appropriate materials and approximate thicknesses and is the basis for initial thermal protection system weight estimates. Metallic thermal protection systems are a key technology for reducing the cost of reusable launch vehicles, offering the combination of increased durability and competitive weights when compared to other systems. Accurate sizing of metallic thermal protection systems requires combined thermal and structural analysis. Initial sensitivity studies were conducted using transient one-dimensional finite element thermal analysis to determine the influence of various design and analysis parameters on thermal protection system weight. The thermal analysis model was then used in combination with static deflection and failure mode analysis of the thermal protection system sandwich panel outer surface to obtain minimum weight configurations at three vehicle stations on the windward centerline of a representative reusable launch vehicle. The coupled nature of the analysis requires an iterative analysis process, which is described. Findings from the sensitivity analysis are reported, along with preliminary designs at the three vehicle stations considered.

Nomenclature

d_e	=	honeycomb cell size, ft
d_g	=	gas collision diameter, ft
H_g	=	gas enthalpy, Btu/lbm
H_{rec}	=	recovery enthalpy, Btu/lbm
h	=	heat transfer coefficient, lbm/ft$^2 \cdot$ s
K_B	=	Boltzmann constant, Btu/R
k_g	=	gas thermal conductivity, Btu/ft-s-°R
k_g^*	=	temperature-dependent gas thermal conductivity for air, Btu/ft-s-°R
k_{rad}	=	equivalent conductivity, radiation in honeycomb core, Btu/ft-s-°R
L	=	diagonal length of thermal protection system (TPS) panel, ft
L_e	=	enclosure characteristic length, ft
L_h	=	honeycomb thickness, ft
Pr	=	Prandtl number
$p_{\text{atmospheric}}$	=	atmospheric pressure at current altitude, lbf/ft^2
p_e	=	pressure in enclosure, lbf/ft^2
$p_{\text{local static}}$	=	local static-normal aerodynamic pressure, lbf/ft^2
q	=	integrated heat load, Btu/ft^2
$\dot{q}$	=	heat flux, Btu/ft$^2 \cdot$ s
T_{av}	=	average temperature in rod element, °R
T_e	=	temperature in enclosure, °R
T_{surf}	=	TPS surface temperature, °R
α	=	accommodation coefficient
γ	=	specific heat ratio for air
$\Delta p_{\text{aerodynamic}}$	=	aerodynamic pressure differential, lbf/ft^2
$\Delta p_{\text{rms, acoustic}}$	=	rms acoustic pressure differential, lbf/ft^2
$\Delta p_{\text{ultimate, TPS+}}$	=	maximum inward pressure differential, lbf/ft^2
$\Delta p_{\text{ultimate, TPS−}}$	=	maximum outward pressure differential, lbf/ft^2
ε	=	emissivity
λ	=	mean free path, ft
σ	=	Stefan–Boltzmann constant, Btu/s $\cdot$ ft$^2 \cdot$ °R^4

Received 28 May 2002; revision received 28 April 2003; accepted for publication 6 June 2003.

*Research Engineer, Metals and Thermal Structures Branch, Structures and Materials Competency.
†Aeronautical Engineer.

Introduction

THERMAL protection systems (TPS) on reusable launch vehicles (RLV) are required to be lightweight while providing protection from heating during ascent and reentry and insulation to cryogenic fuel tanks during ground hold. Recent design goals for RLV have called for commercial aircraftlike operations, which further increases the importance of the TPS. To meet these goals, the TPS must not only be a good insulator capable of withstanding cryogenic and reentry temperatures, but it must be durable and easily maintained. To increase RLV operability, the TPS may be required to withstand exposure to rain and hail.

This paper represents one of several reporting on the development of adaptable robust metallic operable reusable (ARMOR) TPS at NASA Langley Research Center.[1−6] ARMOR TPS, as shown in Fig. 1, employs a lightweight metallic structure to encapsulate high-efficiency fibrous insulation and react aerodynamic pressure to the vehicle structure. The goal of ARMOR TPS development is to improve operational features, increase adaptability (by allowing attachment to different tank and structural configurations), and reduce the weight from previous metallic TPS designs.[1,2] Operability can be increased by modification of TPS design parameters such as outer facesheet gauge (to improve resistance to damage from hail, rain, and orbital debris) and standoff distance from the structure or tank (which greatly improves orbital debris impact resistance[3]).

ARMOR TPS is sized herein to meet the insulation and structural requirements resulting from the ground hold cryogenic environment, as well as the ascent and reentry aerothermal heating environments. The defined preliminary design process is used to determine appropriate TPS materials and approximate thicknesses and is used to generate initial TPS weight estimates. The analysis focuses on sizing of the fibrous insulation layer and sizing of the honeycomb sandwich on the ARMOR TPS outer surface. Dimensions for other components are based on work reported by Blosser et al.[1] Insulation layers are sized by the aerothermal heating and cryogenic

Fabricated Panel

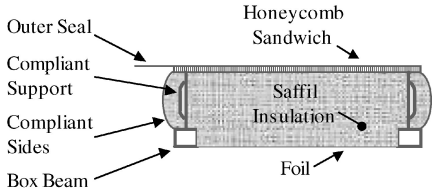

Cutaway View

Fig. 1 As-fabricated and cutaway schematic views of ARMOR TPS.

conditions experienced in the three environments, whereas the honeycomb sandwich panel on the ARMOR TPS outer surface is sized considering aerodynamic pressure, acoustic pressure, and thermal gradients. Thermal performance is dependent on the structure, and the structural response is dependent on the temperatures in the TPS. Therefore, the thermal and structural analyses are coupled, requiring an iterative analysis alternating between thermal and structural analyses. However, the TPS dimensions calculated in the current study have not been sized to meet a specific durability or operability criteria,[2] such as a certain size hail, impact energy, or space debris particle size.

ARMOR TPS Design

Figure 1 shows a fabricated 18 × 18 in. ARMOR TPS panel along with a cross-sectional view showing details of the inner structure. The sandwich panel is exposed to ascent and reentry heating, as well as aerodynamic and acoustic pressure. One of the primary functions of the sandwich panel is to reradiate most of the external aerodynamic heating, dramatically reducing the amount of heat absorbed by the TPS. The honeycomb sandwich panels form an aerodynamic shell that carries aerodynamic pressure on the TPS outer surface. Panel-to-panel gaps are sealed by overhanging metal foil to prevent ingress of hot gases during reentry. Flutter analysis of these seals is reported by Chen and Blosser.[4] Pressure loading is transferred to the box beam picture frame through four corner support brackets.[1] The supports are arranged tangent to a circle about the center of the panel and have low bending stiffness perpendicular to the circle, allowing nearly free in-plane thermal expansion of the sandwich panel while resisting translation and rotation. Bulged, compliant sides, made of thin-gauge metal foil, form the sides of the TPS panel and block the radiative heat transfer path in the panel-to-panel gaps. The interior of the TPS panel is filled with low-density Saffil™ fibrous insulation.[7] A thin-gauge metal foil closes out the bottom of the TPS panel. A mesh covered vent is incorporated into the metal foil backing to allow the TPS internal pressure to be maintained at the pressure beneath the TPS panel.

Preliminary selection of materials for ARMOR TPS was based on the maximum surface temperature experienced. For regions of the vehicle where temperatures are under 1100°F, titanium alloy Ti 1100 was selected. Nickel alloys were used in regions where the maximum surface temperature was between 1100 and 1800–2000°F. In these cases, Inconel 617 is used for the outer honeycomb sandwich panel and compliant sides, and Inconel 718 is used for the thermally compliant supports.

Design of TPS is dependent on the underlying structure. In this analysis, a single-stage-to-orbit RLV is studied that uses foam-filled honeycomb-sandwich semiconformal liquid oxygen (LOX) and liquid hydrogen (LH_2) tanks analyzed in the study by Wang and Johnson.[8] Figure 2 shows the semiconformal tanks, where the LOX tank is forward and the LH_2 tank is aft. The intertank structure

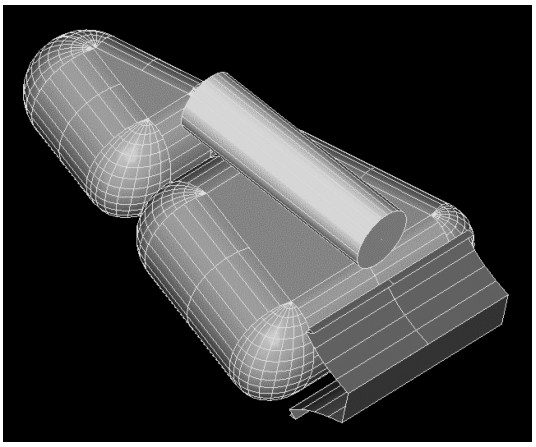

Fig. 2 RLV 003C semiconformal cryogenic fuel tanks.

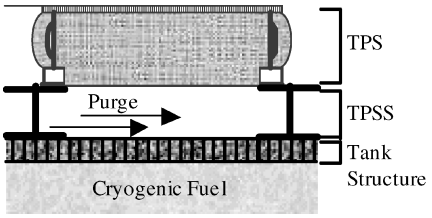

Fig. 3 Cutaway schematic view of TPS mounted on TPSS and tank.

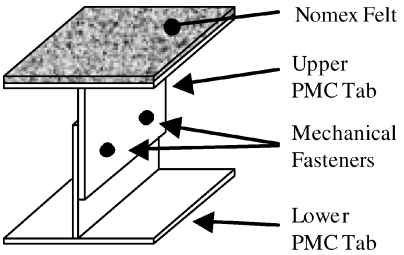

Fig. 4 Schematic of TPSS.

is not shown. The sandwich panel uses graphite epoxy facesheets with Korex© honeycomb filled with TEEK[9] cryogenic foam. The cryogenic foam is used to limit heat flow into the tank during ground hold and prevent air liquefaction in the gap between the TPS and tank during the vehicle ground hold and ascent conditions. The TPS bottom corners are mechanically attached to a TPS support system (TPSS), which is bonded to the tank wall (Fig. 3). A TPSS is used to attach the TPS to the tank structure, while accommodating differences in shape between the outer mold line of the vehicle and the tank, and to form a cavity for purging the system.

Purging is performed during vehicle ground hold before launch and also after landing. Purging is performed with gaseous nitrogen during vehicle ground hold to reduce heat flow into the cryogenic fuel tank and to neutralize any potential tank leaks. Air purging after landing is assumed to be a standard operational procedure and is performed using blowers attached 30 min after vehicle touchdown to cool the tank and support structure. The effect of purge initiation time was studied, including purging while the RLV is still airborne via an air scoop. In addition to forced purging before launch and after landing, the cavity between TPS and tank will be vented during ascent and reentry to allow cavity pressure to equilibrate with atmospheric pressure. It is likely that cavity pressure will require time to equilibrate, resulting in a pressure lag effect. However, RLV venting data were not available, and so the pressure equilibration was assumed to occur instantaneously. In addition, any convective heat transfer phenomena related to venting is neglected in the thermal analysis. The venting assumptions made for thermal and structural analysis are deemed adequate for preliminary sizing of TPS.

Figure 4 is a schematic of the TPSS used in this study, which is composed of two graphite epoxy tabs. The lower tab is bonded to

the tank wall, and the upper tab is then mechanically attached to the lower tab. A felt layer is bonded to the upper surface of the upper tab. The 3×3 in. area on the upper tab surface is used to attach the corners of four adjacent TPS panels. If necessary, the upper tab can be made out of a higher temperature material to reduce the amount of insulation required.

Analytical Method

Aerothermal Environment and Trajectory

Vehicle load, aerothermal environment, and trajectory information was obtained from Dorsey et al.[2] for a RLV lifting-body configuration designated 003c. These data were used to determine outer surface heating and pressure differential loads acting on the outer honeycomb sandwich panel. Three vehicle stations were chosen along the windward centerline for analysis, STA 264, STA 827, and STA 1238, where numeric values represent distance from the vehicle nose in inches. Figure 5 shows the location of the vehicle stations relative to the cryogenic fuel tanks. Station 264 is on the LOX tank near the nose of the vehicle. Stations 827 and 1238 are on the LH_2 tank, where STA 827 is near the middle of the RLV and STA 1238 is near the engines. Aerothermal heating rates[2] are shown as a function of time for the three vehicle stations in Fig. 6. STA 264 was selected because it experiences significant reentry heating. STA 827 is roughly half the vehicle length from the nose and is representative of the vehicle windward acreage area. Finally, STA 1238 was selected because it is near the engines, where high acoustic loading occurs during ascent. Although plume heating can be significant in the design of TPS panels near the engines, it was neglected in this study because the loads were not available.

Aerothermal convective heating was calculated using the equation

$$\dot{q} = h(H_{\text{rec}} - H_g) \tag{1}$$

where h and H_{rec} are time-dependent quantities obtained from the aerothermal environment data. H_g is the gas enthalpy at the temperature of the outer surface and is calculated using the empirical equation

$$H_g = 0.2345T_{\text{surf}} + (9.786E-6)T_{\text{surf}}^2 + 943.6/T_{\text{surf}} - 1.57 \tag{2}$$

Using the recovery enthalpy boundary condition is more accurate than applying a constant temperature heat flux because the influence of TPS surface temperature is included.

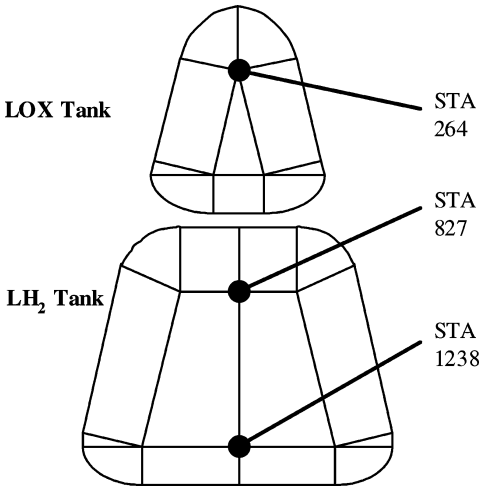

Fig. 5 Location of vehicle stations studied relative to cryogenic fuel tanks.

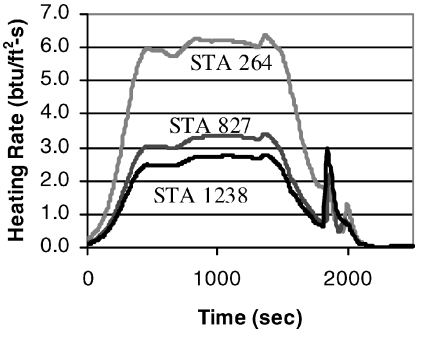

Fig. 6 Heating rates at the vehicle stations investigated.

Thermal Sensitivity Studies

Thermal sensitivity studies were conducted to determine the effect of key assumptions and parameters on TPS insulation requirements and weight. The areas studied were purging during ground hold, reentry purge initiation time, reentry initial temperature, and TPSS temperature limit. A one-dimensional transient heat transfer finite element model, including elements to model the effects of heat shorts, was created for use in the sensitivity studies and for later use in the sizing analysis. Studies by Blosser have shown that one-dimensional models can reasonably predict temperatures in TPS systems.[10]

Thermal Finite Element Model

Figure 7 shows a diagram of the thermal finite element model of the TPS/TPSS/tank system. The TPS/TPSS/tank system is shown schematically in Fig. 3. In the Fig. 7 model diagram, surfaces are depicted by open circles and were used to apply boundary conditions and keep track of surface-related quantities, such as coating emissivity and surface area. Nodes are represented by filled circles, and rod heat transfer elements are represented by lines.

The honeycomb sandwich on the TPS outer surface was modeled using three rod heat transfer elements in parallel, along with increased thermal capacitance at the end nodes to account for facesheet thermal mass. The three elements were used to model solid conduction through the core, gas conduction in the enclosed honeycomb, and radiative heat transfer between the outer and inner facesheets and the core, respectively. The gas thermal conductivity was determined using[11]

$$k_g = k_g^* \Big/ \left[1 + 2\left(\frac{2-\alpha}{\alpha}\right)\left(\frac{2\gamma}{\gamma+1}\right)\left(\frac{1}{Pr}\right)\left(\frac{\lambda}{L_e}\right)\right] \tag{3}$$

In this work, the characteristic length L_e is assumed to be the core height. The mean free path λ is given by

$$\lambda = K_B T_e \Big/ \sqrt{2}\pi d_g^2 p_e \tag{4}$$

For use with the finite element model, T_e was taken to be T_{av}, and p_e was assumed to equal $p_{\text{atmospheric}}$.

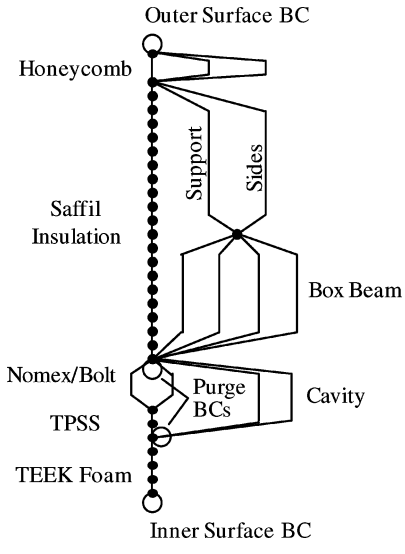

Fig. 7 Thermal finite element model of TPS/TPSS/tank system.

Radiation inside the honeycomb core was approximated using a rod element with an equivalent conductivity calculated using the equations developed by Swann and Pittman[12]:

$$k_{\text{rad}} = 4\zeta\sigma T_{\text{av}}^3 L_h \tag{5}$$

where ζ is given by

$$\zeta = 0.664(\beta + 0.3)^{(-0.69)}\varepsilon^{1.63(\beta+1)^{(-0.89)}} \tag{6}$$

In Eq. (6), ε is a uniform, constant emissivity value inside the honeycomb, and β is given by

$$\beta = L_h/d_e \tag{7}$$

The primary mode of heat transfer through the TPS is through the Saffil fibrous insulation layer, due to its large area. Saffil thermal conductivity is highly pressure dependent, and so it is necessary to model both temperature and pressure dependency of the insulation layer material properties.

In addition to heat transfer through the insulation, the heat shorts resulting from the compliant sides and thermally compliant supports were included. Also, a model of the box beam on the lower surface of the TPS was included that uses four elements in parallel to simulate solid conduction through the box beam sides, solid conduction through the mechanical fasteners, gas conduction, and parallel plate radiation.

The TPS panel rests on a Nomex felt pad at each corner and is mechanically fastened to the TPSS. The interface between TPS panel and TPSS was modeled with two solid conduction elements connected in parallel, one representing the Nomex pad and the other representing mechanical fasteners. The TPSS is modeled with two solid conduction elements connected in series. A cavity is formed between the back of the TPS panel and the outer surface of the tank. Heat transfer across the cavity was modeled with two elements in parallel, one modeling gas conduction in an enclosure and the other modeling radiation between infinite parallel plates. Finally, the foam-filled honeycomb-sandwich tank structure was modeled with four elements in series, representing solid conduction through the cryogenic foam and honeycomb core. The thermal capacitance of the end nodes was increased to account for facesheet thermal mass.

Thermal Load Cases

The boundary conditions for the thermal model were varied to represent the thermal conditions expected during the RLV flight cycle. Three transient thermal load cases were defined: ground hold, ascent, and reentry.

Ground hold analysis was initiated with a uniform initial temperature of 70°F. The cavity between the back of the TPS panel and the outer surface of the sandwich tank is purged with gaseous nitrogen. This was simulated by applying convection boundary conditions to the surfaces marked purge BCs in Fig. 7. Purge temperature was assumed to be −160°F. An empirically calculated heat transfer coefficient of $1.0E-3$ lbm/ft$^2\cdot$s was used to represent forced convection heat transfer, based on the work reported in Ref. 13. This corresponds to an approximate flow rate of 3 ft/s. The purge boundary condition drives the node at which it is applied to within a few degrees of the purge gas temperature, effectively acting like a prescribed temperature boundary condition, so that increasing flow rate beyond 3 ft/s will not significantly influence the results. A prescribed temperature boundary condition is applied to the surface marked inner surface BC (Fig. 7) to model the effect of cryogenic fuel, where temperatures of −423 and −300°F were used for the LH_2 and LOX tank, respectively. In addition, a convective boundary condition, with heat transfer coefficient of $6.94E-4$ Btu/s$\cdot$ft$\cdot$°R is applied to the surface outer surface BC (Fig. 7), simulating convection to ambient air at 70°F. The heat transfer coefficient represents typical launch pad conditions.[14] Steady-state conditions were calculated for ground hold conditions. The cryogenic foam layer was sized to limit heat flux into the tank under steady-state conditions. Then, in the final 30 min before launch, the cryogenic purge temperature is raised to −110°F. In a previous study,[13] it was shown that raising the purge temperature shortly before ascent reduces the required cryogenic foam thickness. Increasing the purge temperature warms the cavity between the TPS and tank, which helps to delay the cooling of these surfaces below air liquefaction temperature during ascent, when there is no purging. It is assumed that the increased heat flux into the tank due to raising the purge temperature for 30 min before launch will be acceptable.

The final temperatures from the ground hold analysis were used as the initial temperatures in the ascent load case. In the ascent load case, the purge boundary condition was removed. The same cryogenic boundary condition on inner surface BC (Fig. 7) used in the ground hold load case was used in the ascent load case. Finally, aerothermal heating and radiation to space boundary conditions are applied on the surface labeled outer surface BC (Fig. 7). Data for calculation of aerothermal heating on the TPS outer surface were obtained from the RLV 003c ascent aerothermal data file.[2] Radiation to space was modeled assuming a constant emissivity of 0.86 and 0.8 for TPS with an Inconel 617 and titanium outer honeycomb-sandwich panel, respectively.

The reentry load case generally assumes a uniform initial temperature of 70°F; however, the significance of the initial temperature is investigated in one of the sensitivity studies. Aerothermal heating and radiation to space boundary conditions are applied on the outer surface BC (Fig. 7) surface. All other surfaces were adiabatic. As with the ascent load case, emissivities of 0.86 and 0.8 are assumed for TPS with Inconel 617 and titanium outer honeycomb-sandwich panels, respectively. It takes approximately 43 min for the RLV to touchdown; however, peak temperatures in the tank wall often occur after touchdown. For this reason, it is necessary to extend analysis to simulate the vehicle sitting on the runway. At 43 min, the boundary condition applied to outer surface BC (Fig. 7) is changed from aerothermal heating and radiation to a convection boundary condition with air temperature set at 70°F. It was assumed that air purging is initiated in the cavity region 30 min after touchdown to cool down the TPS and tank, with 30 min being an estimate of a reasonable amount of time to hook up ground–based blowers to the RLV. Because purging is performed in the area of the TPS/tank system that will be most sensitive to overheating, that is, the TPSS and the tank wall, it is assumed that purging works very quickly to reduce temperatures. The analysis is, therefore, concluded at the initiation of purging. Sensitivity studies were performed to assess the benefits of performing reentry purging more quickly after touchdown, or even while the RLV was traveling at subsonic speeds via an air scoop, and will be reported in the Results section.

Insulation Sizing Criteria

Both the Saffil insulation thickness and the foam-filled honeycomb core thickness were sized using iterative thermal analyses. Saffil insulation thickness was minimized with constraints that temperature limits in the TPS, TPSS, and tank were not exceeded during ascent or reentry load cases, resulting in at least one critical node with temperature equal to a temperature constraint (within a ±5°F tolerance). Temperature limits for all of the materials in the system were considered; however, the Saffil insulation thickness was sized by the 300°F temperature limit of the TPSS and tank. The foam-filled honeycomb tank thickness was optimized such that heat flux into the cryogenic fuel was under 0.01 Btu/s$\cdot$ft^2 and air liquefaction was prevented during ground hold and ascent. The heat flux constraint is based on conservative estimates of heat flux allowed into the shuttle external fuel tank.[13] Pressure-dependent air liquefaction temperature was calculated for ascent conditions. The effect of pressure-dependent air liquefaction temperature during ascent can become an important consideration when purging is performed during ground hold.[13] The thickness of the foam-filled honeycomb determined by structural sizing[8] was the minimum thickness allowed for thermal sizing.

Loads Table Generation

Critical combinations of thermal and structural loads at several times during ascent and reentry were chosen as the design loads for

Table 1 Representative loads at STA 1238 along RLV windward centerline

Parameter	Load cases							
	Liftoff	Ascent maximum Fn	Ascent maximum Δp	Ascent maximum ΔT	Ascent maximum ax	Entry maximum ΔT	Entry maximum $\dot{q}$	Entry maximum Δp
Time, s	6	52	45	130	126	2275	485	1870
Mach	0.05	0.79	0.68	4.20	4.20	1.10	26.90	6.75
$p_{\text{local\_static}}$, psia	$1.46E+01$	$6.90E+00$	$8.54E+00$	$9.10E-02$	$9.10E-02$	$3.43E+00$	$3.82E-02$	$3.06E-01$
$p_{\text{atmospheric}}$, psia	$1.46E+01$	$6.85E+00$	$8.47E+00$	$9.10E-02$	$9.10E-02$	$3.31E+00$	$9.30E-05$	$3.10E-02$
Vehicle_ax, g	$1.38E+00$	$1.55E+00$	1.59+00	$3.00E+00$	$3.00E+00$	$0.00E+00$	$-1.5E-02$	-0.3944
Vehicle_ay, g	$0.00E+00$	$0.00E+00$	$0.00E+00$	$0.00E+00$	$0.00E+00$	$0.00E+00$	$0.00E+00$	0
Vehicle_az, g	$6.10E-04$	$-6.60E-02$	$-1.63E-02$	$6.10E-02$	$6.10E-02$	$0.00E+00$	$-1.70E-01$	-1.646
T_{surf}, °F	60	43	44	285	272	71	1037	1035
$T_{\text{inner\_facesheet}}$, °F	47	43	44	84	76	427	855	890
$T_{\text{bbeam\_top}}$, °F	−100	−98	−98	−94	−94	316	106	267
$T_{\text{bbeam\_bottom}}$, °F	−106	−99	−100	−95	−95	315	80	261
$T_{\text{tpss\_top}}$, °F	−107	−106	−106	−102	−102	286	74	218
$T_{\text{tpss\_mid}}$, °F	−112	−112	−112	−113	−113	207	71	142
$T_{\text{tpss\_bot}}$, °F	−115	−121	−120	−129	−128	255	72	182
$T_{\text{tank\_outer}}$, °F	−115	−121	−120	−129	−128	255	72	182
$T_{\text{tank\_inner}}$, °F	−417	−418	−418	−418	−418	120	70	91
$\Delta p_{\text{aerodynamic}}$, psia	$5.80E-02$	$3.84E-01$	$5.84E-01$	$0.00E+00$	$0.00E+00$	$1.24E-01$	$3.81E-02$	$2.75E-01$
$\Delta p_{\text{rms,acoustic}}$, psia	$9.94E-01$	$2.96E-02$	$2.44E-02$	$9.90E-03$	$9.90E-03$	$1.23E-02$	$4.26E-04$	$8.68E-03$
$\Delta p_{\text{ultimate,TPS+}}$, psia	$4.26E+00$	$6.62E-01$	$9.21E-01$	$4.16E-02$	$4.16E-02$	$2.26E-01$	$5.51E-02$	$4.21E-01$
$\Delta p_{\text{ultimate,TPS-}}$, psia	$-4.09E+00$	$4.13E-01$	$7.16E-01$	$-4.16E-02$	$-4.16E-02$	$1.22E-01$	$5.16E-02$	$3.48E-01$

this study. The design loads for STA 1238 are shown in Table 1. Load cases were defined at the time of occurrence of the following phenomena during ascent: liftoff, maximum normal force on launch vehicle, maximum pressure differential across honeycomb sandwich panel, maximum thermal gradient across honeycomb-sandwich panel, and maximum vehicle axial acceleration. Reentry cases were maximum thermal gradient across honeycomb-sandwich panel, maximum TPS surface heat flux, and maximum pressure differential across honeycomb-sandwich panel. Each load case includes temperatures, atmospheric pressure, static normal pressure acting on the TPS surface, and vehicle accelerations. Acoustic pressure is due to engine acoustics and aerodynamic noise.[2]

Pressure differentials acting on the TPS outer honeycomb-sandwich panel were determined using the equations

$$\Delta p_{\text{ultimate,TPS+}} = 1.4(\Delta p_{\text{aerodynamic}} + 3\Delta p_{\text{rms,acoustic}}) \tag{8}$$

$$\Delta p_{\text{ultimate,TPS-}} = 1.4(\Delta p_{\text{aerodynamic}} - 3\Delta p_{\text{rms,acoustic}}) \tag{9}$$

where $\Delta p_{\text{ultimate,TPS+}}$ and $\Delta p_{\text{ultimate,TPS-}}$ represent the maximum inward and outward pressure differential expected from the combination of aerodynamic pressure and three standard deviations of acoustic pressure, acting in either the positive or negative direction. A factor of safety of 1.4 is applied to the loads.

The ARMOR TPS design forms an aerodynamic shell that carries aerodynamic pressure on the TPS outer surface. The inside of the TPS panel is vented to local pressure beneath the TPS. This local subsurface pressure depends on the internal vehicle geometry and venting scheme. These details were not available for the current study, and so the TPS internal pressure was assumed to equal local atmospheric pressure. The assumption that TPS internal pressure equals local atmospheric pressure allows calculation of $\Delta p_{\text{aerodynamic}}$ using the formula

$$\Delta p_{\text{aerodynamic}} = p_{\text{local\_static}} - p_{\text{atmospheric}} \tag{10}$$

where $p_{\text{local\_static}}$ is the inward acting component of local aerodynamic pressure and $p_{\text{atmospheric}}$ is the local atmospheric pressure at the current vehicle altitude. A positive value indicates inward acting pressure.

Structural Model

A structural finite element model was developed to calculate deflection and loads for localized failure analysis of the outer honeycomb sandwich panel. The model consisted of outer honeycomb sandwich panel modeled with composite shell elements, thermally compliant supports modeled with bar elements, and box beam frame modeled with bar elements. Figure 8 shows the resulting structural finite element model. The model is constrained at points A, B, C, and D, as shown in Fig. 8. All degrees of freedom, except for z rotational freedom, were fixed at point A. Points B and C both had z rotational freedom; in addition point B had translational freedom in the x direction and point C had translation freedom in the y direction. Point D was given translational freedom in the x and y directions, as well as z rotational freedom. All other degrees of freedom at points B, C, and D were fixed. The boundary conditions represent mechanical attachment to expansion slots.[1] Uniform pressure loading was applied on the sandwich outer surface, and temperatures were applied over the entire model. A thermal gradient is applied through the thickness of the composite shell elements. Temperatures and pressure differentials were obtained from the loads table at specific times of interest. Temperature-dependent properties were used for Inconel 617, Inconel 718, and Ti 1100 (Refs. 15–17). Material properties were modified for Inconel 617 to account for the effect of brazing. The most significant effect due to brazing was reduction of room temperature elongation to failure by nearly an order of magnitude.

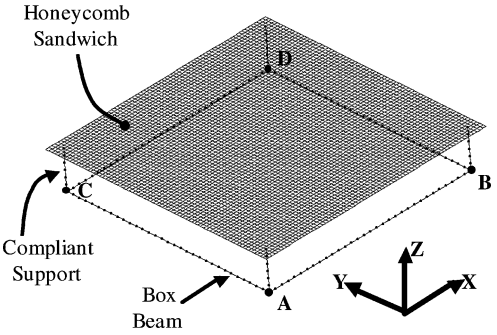

Fig. 8 TPS panel model used in linear static analysis.

Iterative Sizing Method

Thermal–mechanical sizing of the TPS panel was performed following the logic shown in Fig. 9. The process consists of the following steps: 1) making an initial estimate of design parameters, 2) performing iterative transient thermal analyses to size insulation layers, 3) creating a loads table from thermal analysis results and vehicle data, 4) performing static deflection analysis of the outer honeycomb sandwich, and 5) performing local failure analysis of the outer honeycomb sandwich. There are two primary sizing loops in the process: An inner loop occurs in the structural sizing of the

Table 2 Tank wall parameters[8]

Vehicle station	Facesheet thickness, in.	Core thickness, in.
264	0.0750	0.646
827	0.0786	0.504
1238	0.060	0.820

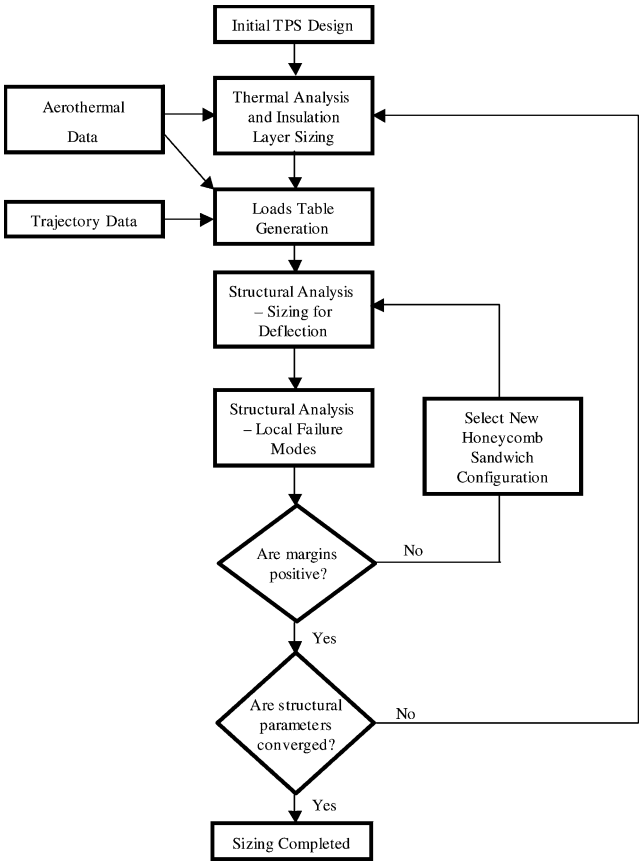

Fig. 9 Thermal-mechanical sizing process.

honeycomb sandwich to determine the minimum-weight design that satisfies both deflection and local failure criteria; the outer loop is used for convergence of the structural parameter values estimated in the thermal analysis with those obtained through structural analysis. This process has to be repeated for each location on the vehicle to be analyzed.

Several structural components were designed in a companion study[1]: thermally compliant supports, box beam, and TPS support structure. In addition, the tank structure was optimized in the work by Wang and Johnson,[8] with relevant results shown in Table 2, where facesheets are IM7/977-2 graphite epoxy and the core is 4.5 lb/ft^3 Korex with 3/16-in. cell size, filled with TEEK cryogenic foam. Potential weight savings can be achieved by sizing TPS insulation and honeycomb sandwich iteratively with the mentioned structural components and tank, however, for the current preliminary design the components were sized separately.

To start the sizing process shown in Fig. 9, an initial estimate of insulation and structural parameter values was made based on previous experience analyzing TPS. Thermal analysis and sizing of insulation thickness is then performed using the thermal finite element model, as described earlier.

Next, a loads table was generated. Structural loads had been previously calculated as a function of time for ascent and reentry. Results of the thermal analysis were used to complete or update the loads table. The thermal analysis not only determined the key temperatures for all load cases, it also determined times associated with some of the critical load cases, for example, maximum-temperature gradient. These times were then used to identify the associated structural loads to complete the load table. Linear static deflection analysis of the honeycomb panel due to thermal gradients and pressure differentials was performed with NASTRAN. Deflection limits were imposed to prevent boundary-layer transition at high Mach numbers and to prevent permanent compaction of fibrous insulation. Excessive deflection of the TPS outer surface can result in an early transition of boundary layer from laminar to turbulent in the external aerodynamic flow, thereby greatly increasing the external heating. For this reason, at velocities greater than Mach 5.0, a deflection limit based on Table 3 is imposed on the honeycomb-sandwich panel.[2] In Table 3, L is the diagonal length of the TPS panel. The second deflection limit, imposed to prevent permanent insulation compaction, is in effect for all load cases and requires that the TPS outer sandwich panel deflection not exceed 10% of the total TPS panel thickness. Sandwich panel deflection may also result in localized heating enhancement, which was not accounted for in this study.

Table 3 Transition-based deflection limits[2]

Location	Deflection/L
Leading edge	0.01
Windward forebody	0.01
Windward aft body	0.015
Leeward forebody	0.015
Leeward aft body	0.025

Two different materials were considered for the outer honeycomb sandwich: Inconel 617 and Ti 1100. Material selection was based on maximum temperature reached. A range of facesheet thickness (0.006–0.016 in., in increments of 0.001 in.) and honeycomb depth (0.25–1.00 in., in increments of 0.05 in.) was considered. The 0.006-in. facesheet thickness represents minimum facesheet gauge based on manufacturing considerations. A higher minimum gauge may be required to meet future criteria for impact from hail, flying through rain, orbital debris, etc.[2] Also, four different honeycomb specifications (ribbon thickness by cell size) were considered: $0.002 \times 1/8, 0.002 \times 3/16, 0.002 \times 1/4$, and $0.002 \times 3/8$ in. A routine was created to analyze and determine automatically the weight of all honeycomb designs, a total of 704 structural designs, in the design space defined by the sandwich panel variables. From this, a table of candidate designs, sorted by increasing weight, was created for each material (Inconel 617 and Ti 1100).

The lowest weight honeycomb-sandwich panel that passed deflection criteria was then analyzed to check for localized failures. A commercial structural sizing program, Hypersizer®, was used to check local honeycomb stress failure criteria including in-plane tensile failure and in-plane shear failure of the facesheets, intracellular dimpling of the face sheets, transverse shear failure of the core, and core crushing. Documentation for Hypersizer is unpublished, but is available from Collier Research, Inc., at URL: http://www.collier-research.com. At this point in the thermal/structural sizing, the first decision box in Fig. 9 had been reached. If the candidate honeycomb sandwich passed the localized failure criteria, analysis proceeded to the second decision box. Otherwise, the next heavier honeycomb sandwich that passed the deflection criteria was selected and checked for localized failure. This inner loop was repeated until an acceptable design was found.

Next, the structural parameters used in the thermal analysis were compared to the structural parameters determined from the structural analysis, as illustrated in the second decision box, shown in Fig. 9. If the parameters were within tolerance, the analysis for this vehicle station was complete. Otherwise, the thermal analysis was repeated with the updated structural parameters. Tolerance was defined as ± 0.002 in. for facesheet gauge and ± 0.05 in. for honeycomb depth. In all cases, honeycomb gauge and honeycomb cell size was matched exactly between thermal and structural analysis. For the analyses performed in this study, two to three iterations were required on the outer sizing loop to reach convergence.

Results

Two different sizing studies were completed. The first study was a thermal sensitivity study to determine the effect of several analysis

assumptions, and the second study combined thermal and structural analysis to size TPS panels.

Thermal Sensitivity Study

A sensitivity study was performed using only the thermal analysis to size the thicknesses of the TPS and cryogenic insulation. This simplified analysis was used to investigate the importance of analysis assumptions and design decisions relating to 1) ground hold purging, 2) reentry purging initiation time, 3) assumed initial reentry temperature, and 4) increasing TPSS temperature limit. Structural parameters were held constant throughout the thermal sensitivity study, with emphasis on determining the influence of the stated changes on Saffil and cryogenic foam-filled honeycomb layer weight.

Weights directly related to insulation layer thickness (Saffil, cryogenic foam insulation, compliant supports and sides, and cryogenic fuel tank honeycomb core) were calculated for typical TPS designs and compared to the overall weight of the TPS, TPSS, and tank sandwich panel. As shown in Fig. 10, the weight directly related to insulation layer thickness amounts to between 34 and 39% of the overall TPS/tank system weight, depending on which vehicle location is examined.

Figure 11 shows a comparison of insulation weight of systems that were purged during ground hold with unpurged systems. At STA 264 and STA 1238 purging had no effect on system weight. This is due to the constraint that cryogenic foam insulation thickness be greater than or equal to the core thickness determined by structural analysis of the tank. At STA 827, purging resulted in an increase in required cryogenic foam thickness to prevent violation of the constraint limiting heat flux into the tank. Insulation requirements can be reduced at this vehicle station by reducing the purge temperature.

Most analyses assumed that reentry purging was performed 30 min after vehicle touchdown, which would be accomplished by attaching external blowers to the RLV to purge the cavity between the TPS and tank. In Fig. 12, the effect of purging at an earlier time is examined. Times of 4365 and 3465 s correspond to 30 and 15 min. after touchdown, respectively. Purging at 2360 s is accomplished while the RLV is still in the air at subsonic velocity via an air scoop. As shown in Fig. 12, there is only a small benefit from purging early.

The initial temperatures of the TPS and tank are often not well known at a preliminary design stage, yet they can be important for sizing insulation required for reentry. Figure 13 shows that there is significant sensitivity of TPS insulation-related weights to assumed initial temperature. This information may be useful from an operations standpoint because it indicates that measures taken on orbit to reduce vehicle temperature before reentry will significantly reduce TPS weight. Note that there is a large jump in insulation-related weight between assumed initial reentry temperatures of 70 and 250°F. The jump in insulation weight results from that reentry insulation sizing is being driven by the 300°F temperature limit of the TPSS and tank structure. By the increase of the initial temperature from 70 to 250°F, the allowed change in temperature of the TPSS and tank is reduced from 230 to 50°F, which means that

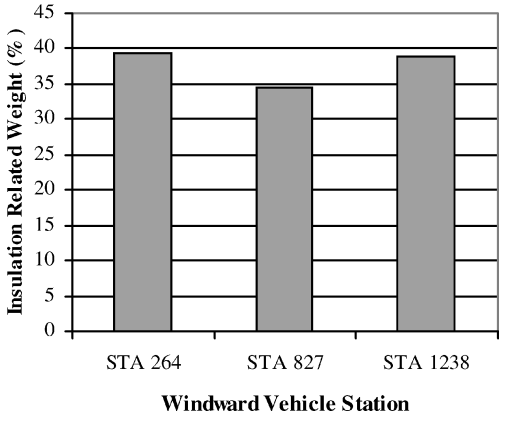

Fig. 10 Percentage of TPS/tank weight directly influenced by insulation thickness.

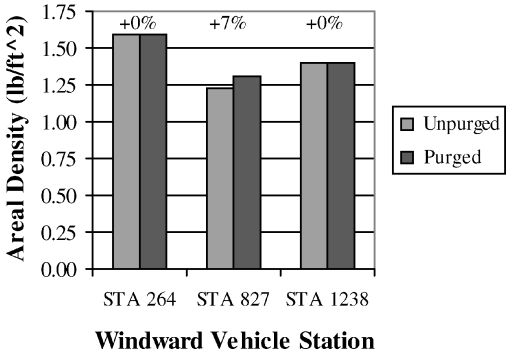

Fig. 11 Comparison of insulation related weight of unpurged vs purged systems.

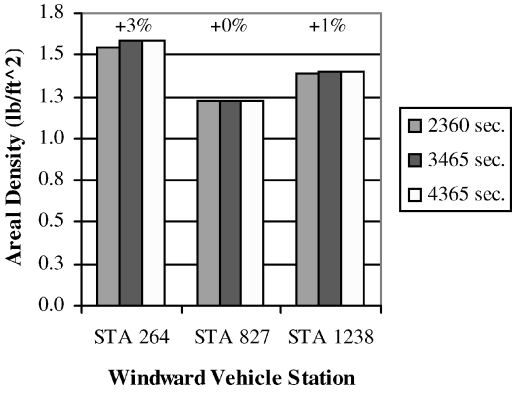

Fig. 12 Effect of early reentry purge on insulation-related TPS/tank weight.

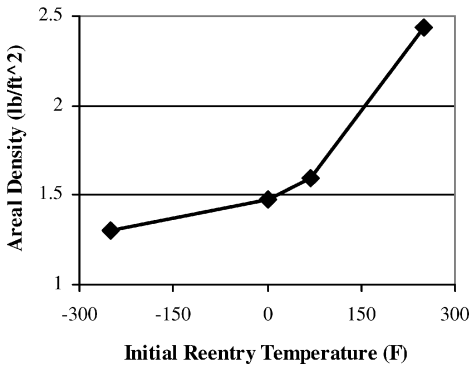

Fig. 13 Effect of assumed initial reentry temperature on insulation-related TPS/tank weight.

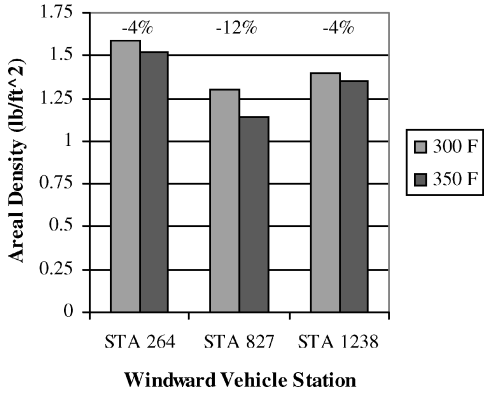

Fig. 14 Effect of TPSS temperature limit on insulation-related TPS/tank weight.

Table 4 Insulation sizing summary

Case	Vehicle station	Sandwich panel material	Maximum surface temperature, °F	Reentry integrated heat load, Btu/ft^2	Reentry insulation		Cryogenic insulation	
					Saffil insulation thickness, in.	Sized by	TEEK foam thickness, in.	Sized by
1	264	Inconel	1514	8925	3.08	TPS Support	0.646	Tank minimum Thickness
2	827	Inconel	1225	4724	2.10	TPS Support	0.62	Heat flow
3	827	Titanium	1224	4724	1.98	TPS Support	0.62	Heat flow
4	1238	Titanium	1140	3984	1.89	TPS Support	0.82	Tank minimum Thickness

Table 5 Structural sizing summary

Case	Vehicle station	Material	Honeycomb properties, in.			Facesheet properties		Sizing information		
			Thickness	Cell size	Gauge	Material	Thickness, in.	Critical deflection load case	Critical local failure load case	Critical local failure mode
1	264	Inconel	0.35	0.25	0.002	Inconel	0.006	Ascent, maximum ΔP	Ascent, maximum ΔP	Intracell dimpling
2	827	Inconel	0.30	0.25	0.002	Inconel	0.006	Liftoff	Liftoff	Intracell dimpling
3	827	Titanium	0.45	0.25	0.002	Titanium	0.006	Liftoff	Liftoff	Intracell dimpling
4	1238	Titanium	0.75	0.25	0.002	Titanium	0.008	Entry, maximum ΔT	Liftoff	Intracell dimpling

Table 6 Representative TPS panel weights calculation, STA 1238

Component	Part weight, lb	Quantity	Total part weight, lb	Component weight, lb
Honeycomb sandwich				1.97
Outer skin	0.41	1	0.41	
Inner skin	0.40	1	0.40	
Braze alloy	0.04	1	0.04	
Core	1.13	1	1.13	
Reentry insulation				0.98
Saffil	0.98	1	0.98	
Box beam				0.42
Hat section	0.20	1	0.20	
Base frame closure	0.14	1	0.14	
Bottom closure	0.08	1	0.08	
Compliant support				0.50
Upper corner	0.05	4	0.19	
Hole plug	0.02	4	0.06	
Bellows	0.01	4	0.05	
Standoff	0.01	4	0.04	
Lower corner	0.04	4	0.15	
Compliant sides				0.09
Side closure	0.02	4	0.09	
Total weight				3.96

Table 7 Assumptions for material properties, STA 1238

Property	Value
Titanium density, lb/in.^{3}	0.16
Saffil density, lb/in.^{3}	0.0017
Ti h/c core density, %	1.63
Ti h/c LID density, lb/in.^{3}	0.32

Table 8 Design parameters, STA 1238

Parameter	Value, in.
Repeat length	18.00
Length of side	17.50
Height of side closure	2.64
Side closure thickness	0.003
Outer H/C core thickness	0.75
Outer facesheet thickness	0.008
Inner facesheet thickness	0.008
Overhanging lip	0.315
Insulation thickness	1.89
Box beam height	0.50
Box beam top width	0.50
Ti/LID layer thickness	0.0002

the heat capacity of the TPSS and tank that can be used to store the absorbed energy during reentry is reduced by a factor of 4.6.

The TPSS and cryogenic fuel tank facesheets were assumed to be made of graphite epoxy with a maximum temperature limit of 300°F. In all analyses, the TPSS temperature limit constraint was active in the sizing of Saffil insulation. It was anticipated that using a material with a higher temperature limit for the TPSS would significantly reduce TPS weight. For this final sensitivity study, the temperature limit of the TPSS was increased to 350°F, which resulted in the tank structure temperature limit becoming the active constraint during Saffil insulation sizing. As shown in Fig. 14, because the tank structure temperature limit constraint was already close to being active, there was only a small weight reduction at STA 264 and STA 1238, with a larger 12% weight reduction at STA 827.

Thermal–Mechanical TPS Sizing

Thermal–mechanical TPS sizing combined thermal analysis with structural and local failure analysis of the outer honeycomb-sandwich panel. Pressure differentials and heating profiles change significantly over the vehicle stations studied, requiring different honeycomb design for each station.

Table 4 shows the results of thermal sizing of the insulation layers at three vehicle stations. Maximum calculated TPS surface temperatures ranged from 1514°F at STA 264 to 1140°F at STA 1238. Inconel 617 TPS was used for STA 264 because the maximum surface temperature is well above the temperature limit of Ti 1100. Two cases were examined at STA 827. Case 2 used Inconel 617 TPS, and case 3 used Ti 1100 TPS. This was done to assess the potential benefits of running Ti 1100 past the material temperature limit. At STA 1238, Ti 1100 TPS was used because the maximum surface temperature is close to the temperature limit of Ti 1100. Reentry insulation ranged from 1.89 to 3.08 in., with all cases being sized by the TPSS temperature limit. Cryogenic insulation thickness ranged from 0.62 to 0.82 in., with sizing driven by either allowable heat flux into the fuel tank during ground hold or minimum structural thickness of the fuel tank sandwich panel.

Table 5 shows results from structural sizing of the TPS honeycomb sandwich panel. In all cases, honeycomb core was selected

Table 9 Component and total weight variation with vehicle station

			Component weight, lb					TPS panel	
Case	Vehicle station	Sandwich panel material	Sandwich panel	Saffil insulation	Box beam	Compliant supports	Compliant sides	Weight, lb	Areal density, lb/ft^2
1	264	Inconel	1.99	1.61	0.42	0.82	0.22	5.05	2.24
2	827	Inconel	1.92	1.09	0.42	0.82	0.15	4.39	1.95
3	827	Titanium	1.32	1.02	0.42	0.50	0.08	3.35	1.49
4	1238	Titanium	1.97	0.98	0.42	0.50	0.09	3.96	1.76

with 0.25-in. cell size and 0.002-in. ribbon gauge. Honeycomb thickness ranged from 0.30 to 0.75 in., depending on vehicle station and material used. Facesheet thickness was normally sized by the minimum material gauge constraint of 0.006 in., but was 0.008 in. at STA 1238.

The sizing information section of Table 5 reports the load cases that produced the worst loading conditions for sizing of the honeycomb panel due to deflection and local failure modes. Critical deflection load case identifies the load case that resulted in the maximum honeycomb panel deflection. Critical local failure load case reports the load case that produced the lowest margins of safety used in sizing for localized failure modes. Finally, critical local failure mode lists the local failure mode with the lowest margin of safety.

Examining the results for STA 264 in Table 5, it can be seen that both the critical deflection and local failure load case were driven by the maximum-pressure differential during ascent (1.76 psia) on the outer TPS surface. This load case occurs 60 s after liftoff.

Cases 2 and 3 were performed at STA 827, with Inconel 617 honeycomb-sandwich panel used in case 2 and Ti 1100 honeycomb-sandwich panel used in case 3. In both cases, the critical deflection and local failure load cases were driven by engine acoustic pressure during the initial seconds of liftoff. The pressure differential on the outer surface was 1.3 psia, primarily due to engine acoustics. Although thicker titanium honeycomb sandwich was required, the titanium sandwich was still significantly lighter than an Inconel 617 sandwich sized for the same load.

Vehicle station 1238 required the thickest outer honeycomb core, 0.75 in. Structural design at this station is interesting in that initial sizing iterations were driven by liftoff acoustics, resulting in increased honeycomb core thickness. However, as the honeycomb core was made thicker, thermal gradients through the core became more significant to panel deflection, until the reentry maximum thermal gradient load case became the structural sizing driver. This load case occurs 38 min into reentry, shortly before touchdown. The thermal gradient is -356°F (resulting in inward concaved panel shape) with minimal aerodynamic pressure. The critical load case for localized failure sizing was still the liftoff condition, due to the 4.26-psia pressure differential, predominantly due to engine acoustics.

Table 6 shows a representative TPS weights calculation at STA 1238 broken down by component. Table 7 lists assumptions for material properties and Table 8 lists design parameters. It is assumed that the honeycomb core and skin are joined using a liquid interface dispersion (LID) technique with properties as listed in Tables 7 and 8. Properties for Ti 1100 were obtained from Ref. 17, and properties for Inconel 617 and Inconel 718 were obtained from Refs. 15 and 16, respectively. Material properties for the Saffil fibrous insulation layer were obtained from Ref. 7. Weights for the box beam, compliant support, and compliant sides components represent nominal weights.[1]

Component and total TPS weights for each case are summarized in Table 9. There is a 13% decrease in TPS panel weight between cases 1 and 2, due to the decreased insulation requirements at STA 827. Case 3 uses Ti 1100 instead of Inconel 617 for the honeycomb sandwich, as well as compliant support and compliant sides components, resulting in a 24% weight reduction. The reduced weight of the honeycomb sandwich contributes to 58% of this weight reduction, with the reduced weight of the compliant support and compliant sides components contributing to 38% of the weight reduction. It is obvious that titanium is preferable at STA 827 if the outer surface can be made to withstand the 1225°F reentry temperature. The severe acoustic pressure and thermal gradients resulting from increasing honeycomb thickness result in a 49% increase in honeycomb-sandwich weight at STA 1238 (case 4). Changes in other component weights are minimal, and overall TPS weight is increased by 18%.

Conclusions

Metallic TPS is an important technology for reducing the cost of future RLV. The ARMOR TPS concept discussed offers potential improvements to the adaptability, robustness, and operability of current reusable TPS. An analysis process suitable for preliminary design of metallic TPS is described, which allows selection of suitable TPS materials, and estimation of insulation and structural thicknesses and TPS weight at selected vehicle locations. In addition, several thermal sensitivity studies were performed to determine the influence of analysis and design parameters on insulation sizing.

Thermal sensitivity studies were conducted with several design and analysis parameters. It was found that ground hold purging at -160°F will increase cryogenic insulation requirements at some vehicle stations. A lower purge temperature would reduce the required cryogenic insulation. In addition, performing reentry purging was not effective in reducing insulation requirements for the initiation times examined. Initial temperature of the TPS and tank on reentry has a large effect on insulation sizing, with initial temperatures greater than 70°F resulting in significant insulation weight penalties. Finally, it was seen that in general increasing the TPSS temperature limit did not significantly reduce TPS weight when tank structure is a epoxy composite.

A sizing process was created for metallic TPS panels using a coupled thermal and structural analysis approach. The process included insulation sizing using the thermal model generated for the sensitivity studies, deflection analysis of the outer honeycomb-sandwich panel using a linear static finite element model, and local failure analysis of the honeycomb panel using Hypersizer. Sizing was performed at vehicle stations 264 (forward), 827 (midbody), and 1238 (aft) along the windward centerline of a lifting-body RLV. In all cases, the Saffil fibrous insulation layer was sized during reentry by the temperature limit of the TPSS. The cryogenic-foam-filled honeycomb core tank wall was sized either by structural loading, using results from Ref. 8, or the constraint on heat flux into the tank during ground hold. At STA 264, near the nose of the RLV, the TPS outer honeycomb-sandwich panel was sized by maximum aerodynamic pressure during ascent. At STA 827, the panel was sized by acoustic loading during liftoff. Finally, at STA 1238, the panel was sized by a combination of acoustic loading during liftoff and thermal gradient induced deflection during reentry. In all cases, the critical local failure mode of the honeycomb sandwich was intracell dimpling of the facesheets.

TPS panel weight decreased from STA 264 to STA 827 due to decreased insulation requirements. If Ti 1100 can be used at temperatures of 1225°F, a significant weight savings can be realized in the region of STA 827. Finally, TPS panel weight increases at STA 1238 due to acoustic pressure and thermal gradients resulting from increased honeycomb thickness.

In conclusion, a useful method was developed for sizing metallic TPS subject to thermal–mechanical loading. The parametric results provide guidance for future metallic TPS designs.

References

[1]Blosser, M. L., Chen, R. R., Schmidt, I. H., Dorsey, J. T., Poteet, C. C., Bird, R. K., and Wurster, K. E., "Development of Advanced Metallic Thermal-Protection-System Prototype Hardware," *Journal of Spacecraft and Rockets*, Vol. 41, No. 2, 2004, pp. 183–194; also AIAA Paper 2002-0504. Jan. 2002.

[2]Dorsey, J. T., Poteet, C. C., Wurster, K. E., and Chen, R. R., "Metallic Thermal Protection System Requirements, Environments, and Integrated Concepts," *Journal of Spacecraft and Rockets*, Vol. 41, No. 2, 2004, pp. 162–172; also AIAA Paper 2002-0502, Jan. 2002.

[3]Poteet, C. C., and Blosser, M. L., "Improving Metallic Thermal Protection System Hypervelocity Impact Resistance Through Numerical Simulations," *Journal of Spacecraft and Rockets*, Vol. 41, No. 2, 2004, pp. 221–231; also AIAA Paper 2002-0912, Jan. 2002.

[4]Chen, R. R., and Blosser, M. L., "Metallic Thermal-Protection-System Panel Flutter Study," *Journal of Spacecraft and Rockets*, Vol. 41, No. 2, 2004, pp. 207–212; also AIAA Paper 2002-0501, Jan. 2002.

[5]Blosser, M. L., "Fundamental Modeling and Thermal Performance Issues for Metallic Thermal Protection System Concept," *Journal of Spacecraft and Rockets*, Vol. 41, No. 2, 2004, pp. 195–206; also AIAA Paper 2002-0503, Jan. 2002.

[6]Bird, R. K., Wallace, T. A., and Sankaran, S. N., "Development of Protective Coatings for High-Temperature Metallic Materials," *Journal of Spacecraft and Rockets*, Vol. 41, No. 2, 2004, pp. 213–220.

[7]Blair, W., Meaney, J. E., and Rosenthal, H. A., "Re-Design of Titanium Multi-Wall Thermal Protection System Test Panels," NASA CR-172247, Jan. 1984.

[8]Wang, J. T., and Johnson, T. F., "Cryogenic Tank Structure Sizing with Structural Optimization Method," AIAA Paper 2001-1599, April 2001.

[9]Weiser, E. S., Johnson, T. F., St. Clair, T. L., Echigo, Y., Kaneshiro, H., and Grimsley, B. W., "Polyimide Foams for Aerospace Vehicles," *High Performance Polymers*, Vol. 12, Feb. 2000, pp. 1–12.

[10]Blosser, M. L., "Advanced Metallic Thermal Protection Systems for Reusable Launch Vehicles," Ph.D. Dissertation, Graduate School of Engineering and Applied Science, Univ. of Virginia, Charlottesville, VA, May 2000.

[11]Daryabeigi, K., "Analysis and Testing of High Temperature Fibrous Insulation for Reusable Launch Vehicles," AIAA Paper 99-1044, Jan. 1999.

[12]Swann, R. T., and Pittman, C. M., "Analysis of Effective Thermal Conductivites of Honeycomb-Core and Corrugated-Core Sandwich Panels," NASA TN D-714, April 1961.

[13]Poteet, C. C., "Groundhold and Reentry Purge Parameter Trade Study," Lockheed Martin Space Operations, Rept. LMES SDSR 99-01, Hampton, VA, Aug. 1999.

[14]Gruszczynski, M. J., Thorp, V. L., Heim, W. J., and Swanson, N. J., "Design, Development, and Test of the Atlas Liquid Hydrogen Propellant Tank Foam Insulation System," AIAA Paper 91-1438, June 1991.

[15]Klopp, W. D., "Inconel 617," *Aerospace Structural Metals Handbook*, 1994 ed., Vol. 5, CINDA/USAF CRDA Handbooks Operation, Purdue Univ., West Lafayette, IN, 1994, pp. 1–34.

[16]Kattus, J. R., "Inconel 718," *Aerospace Structural Metals Handbook*, 1994 ed., Vol. 4, CINDA/USAF CRDA Handbooks Operation, Purdue Univ., West Lafayette, IN, 1994, pp. 1–58.

[17]Hutt, A. J., and Parris, W. M., "TIMETAL-1100 Sheet Properties," *Titanium '92 Science and Technology*, TMS, San Diego, CA, 1993, pp. 2923–2930.

S. A. Bouslog
Associate Editor